Regenerator site selection in nonlinear impairment-aware elastic optical networks

Madushanka Nishan Dharmaweera, Li Yan, Magnus Karlsson, Erik Agrell, and Juzi Zhao

***Abstract*—Potential spectral efficiency gains and transmission reach of traffic connections in elastic optical networks are hindered by the encounter of linear and nonlinear physical-layer impairments. To counter this problem, regenerators are used in elastic optical networks. In this study, we propose a novel regenerator site selection scheme, which accurately accounts for such impairments. Our proposed scheme offers spectral efficiency gains in both small and large networks at different traffic volumes using a limited number of regenerator sites. In addition, we highlight some characteristics of potential regenerator sites in three major networks.**

I. Introduction

The rising popularity of mobile Internet, video streaming, and cloud computing services will increase Internet traffic threefold between the years 2014 and 2019 [1]. To accommodate this growing demand, optical transport networks have to be deployed with the most recent and advanced technologies. Legacy wavelength division multiplexed (WDM) optical transport networks would then gradually evolve into more transmission-rate-flexible, reconfigurable, and high-capacity elastic optical networks (EONs).

Recent advancements in optical technologies have enabled transmission rates in excess of 400 Gb/s and increased the capacity of WDM networks. Yet, due to rigid and coarse-granularity wavelength allocation, WDM technology leads to inefficient capacity utilization, especially in networks serving heterogeneous traffic. Instead of allocating an entire wavelength, in an EON, a traffic connection is only assigned a set of consecutive spectrum slots (i.e., subcarriers) that are appropriately modulated to provide "just enough" bandwidth [2], [3], [28]. As spectrum slots are spaced at a finer granularity (e.g., 6.25 GHz), modulated, and combined to accommodate connections of different bandwidths, EONs significantly reduce capacity waste vis-à-vis traditional WDM networks.

In recent years, EONs have drawn the attention of many researchers. Various routing, modulation, and spectrum allocation (RSA) schemes developed have shown increased spectral efficiency (i.e., capacity utilization) and, therefore, lower resource usage, power consumption, and bandwidth blocking ratio (BBR) [5]–[7]. However, physical-layer impairments (PLI) are shown to have a significant effect on the performance of EONs [2], [8]–[10]. Specifically, due to the accumulation of both linear and nonlinear impairments that arise between co-propagating traffic connections with different modulation formats and bit rates, a connection's signal quality degrades as it travels along its physical path. Resultantly, the received connection may not satisfy the required bit error rate (BER) in a transparent EON. To overcome such PLI and maintain signal quality, a connection can be regenerated at an intermediate node. A transparent EON could thus be transformed into a translucent EON by converting a subset of nodes into regenerator sites. To reduce network cost, it is imperative that regenerator sites are only employed at a few nodes [11], [12].

Regenerator placement in WDM networks has been heavily scrutinized in the past [13]–[18]. In these studies, the authors minimized cost and/or energy consumption of single-line rate, multi-line rate (MLR), or waveband-switched WDM networks by accurately identifying regenerator sites or the number of regenerators. In [12], the authors evaluated the complexity of the regenerator site selection problem of a WDM network and proposed a low-complexity approximation algorithm. Using this approximation algorithm, Xie et al. [17] developed a novel heuristic scheme to find the regenerator sites of a mixed-line rate WDM network.

Although widely studied in WDM networks, regenerator placement is a relatively new and understudied issue in EONs, especially under static traffic conditions [21]. Yet, a handful of studies have shown, through suitable regenerator placement in EONs, impressive results in terms of higher spectral efficiency [19], [25], lower power consumption [22], and lower BBR [20], [23], [24]. For example, the heuristic algorithm in [19] reduces spectrum use by selecting an appropriate number of regenerators at each site. The authors of [20], [23], and [24] reduce BBR by choosing the appropriate number of regenerators at each site in the considered EONs under dynamic traffic conditions. Moreover, the relationship between regenerator site selection and spectrum use in an EON with static traffic demands was analysed in [25].

While the results of such research are promising, a potential limitation is that signal quality degradation due to linear and nonlinear impairments may not have been accurately accounted for. For example, the RSA schemes in [19]–[23], [25] may not accurately account for PLI as the transmission reach (TR) of the different modulation schemes are assumed to be independent of the bit rate and the network topology. The impairment model in [22] accounts for interference from

Parts of this paper has been accepted to be presented at the Optical Fiber Communication Conference (OFC), Anaheim, CA, Mar. 2016.

M. N. Dharmaweera, L. Yan, M. Karlsson, and E. Agrell are with Chalmers University of Technology, SE-41296 Gothenburg, Sweden (e-mail: nishan@chalmers.se). J. Zhao is with the University of Massachusetts-Lowell, MA 01854, United States.

neighboring channels by adding a fixed number of guardbands (GBs), whose width is an integer number of spectrum slots, between co-propagating connections. However, a fixed GB does not rely on the actual network state and, thus, the impairment model may have over- or underestimated the PLI [10]. The transmission distances for different modulation formats and bit rates in [25], which were approximated using the fixed GB-based experimental data of [26], may also not be optimum. Furthermore, due to the inherent complexity of the RSA schemes in [25], they were tested in networks that serve a small number of traffic connections, and not a full traffic matrix. The results in [25] may thus appear to hold only when nonlinear impairments are minimal. Limited modulation conversion capability is another potential limitation of the work in [20], [21]. The majority of prior research has also focused on reducing only the number of regenerators employed, while fewer studies have attempted to reduce the number of regenerator sites [17].

To overcome the aforementioned limitations, it is important to further investigate the issue of regenerator placement in a *realistic impairment-aware* EON. Such a network exists in the work of [10], which developed a state-of-the-art, realistic, impairment-aware (RIA) RSA scheme that uses an accurate, yet tractable, PLI model [27]. That scheme offered spectral efficiency improvements over existing TR-based RSA schemes that use a fixed GB [10].

Therefore, in the current study, we analyze the regenerator placement problem in the realistic impairment-aware EON of [10], using the PLI model of [27], to determine if further spectral efficiency improvements can be attained. We propose a novel regenerator site selection RSA scheme to increase the spectral efficiency of an impairment-aware EON (i.e., RSIE). Our proposed scheme incorporates a realistic and accurate PLI model, considers all-to-all traffic distribution (i.e., a full static traffic matrix), allows both modulation and spectrum conversion, and presents both an optimal solution and heuristic algorithms, thus extending beyond the schemes proposed in the extant literature. To demonstrate the applicability and performance of our proposed scheme to network operators, we assess its performance in networks of different sizes and for different traffic loads. Importantly, we highlight that spectral efficiency can be significantly increased by selectively placing regenerators at a handful of core node sites, which is desirable to minimize network cost.

The remainder of this paper is organized as follows. In Section II, we describe the architecture of a translucent EON and introduce the PLI model. The impact of regenerator site selection is then discussed using an illustrative example. In Section III, the issue of regenerator site selection in an impairment-aware EON is expressed as an RSA problem, which is subsequently formulated using integer linear programming (ILP) and heuristics. In Section IV, we demonstrate the spectral efficiency improvements achieved by our proposed scheme using numerical simulations. Concluding remarks are provided in Section V.

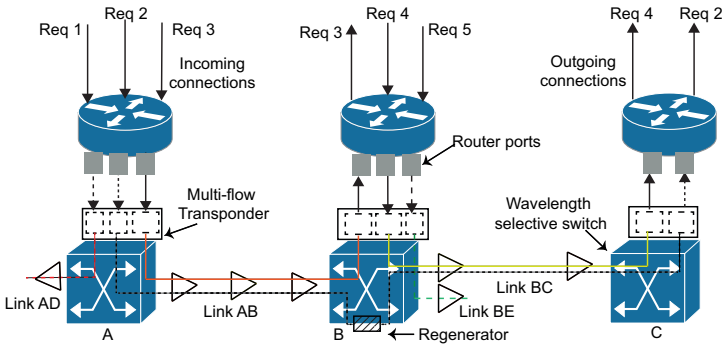

Fig. 1: The schematic of a small section of a translucent EON.

II. System description

In this section, we first describe the architecture of the translucent EON. We then present the PLI model and introduce an approximation method. Lastly, we demonstrate by example, how spectral efficiency can be improved by appropriately selecting regenerator sites.

A. Network architecture

In the network schematic depicted in Fig. 1, traffic connections (i.e., connections/requests/demands) enter the transport layer via router ports and transponders [6], [28]. Each connection is assigned a set of contiguous spectrum slots and a modulation format by the transponders. End-to-end connections are realized using lightpaths set up between transponders of different nodes. These lightpaths travel through optical fibers (i.e., links) that are equipped with amplifiers. A lightpath is switched from one fiber to another by the wavelength-selective switches along its physical routing path.

In a translucent network, certain nodes are equipped with 3R (re-shape, re-time, re-amplify) regenerators. At these sites, an arriving lightpath that has encountered severe degradation is regenerated. A 3R regenerator closely resembles a back-to-back transponder [22], and is, hence, capable of converting the modulation format and the spectrum of a lightpath [20], [22], [25].

B. Physical-layer impairment model

The PLI model used in this study is derived from the Gaussian noise (GN) model presented in [27] and [29], which accurately accounts for both linear and nonlinear impairments. For every connection i, the signal-to-noise ratio (SNR) is expressed as

$$\mathrm{SNR}_i = \frac{G}{G_{\mathrm{ASE}_i} + G_{\mathrm{NLI}_i}} \tag{1}$$

where G, G_{ASE_i}, and G_{NLI_i} denote the power spectral density (PSD) of the signal, the PSD of the amplified spontaneous emission (ASE) noise, and the PSD of the noise from nonlinear impairments (NLI), respectively. To successfully transmit connection i along the designated physical path, the condition $\mathrm{SNR}^k \leq \mathrm{SNR}_i$ has to be satisfied when connection i is assigned modulation format k and SNR^k represents the SNR

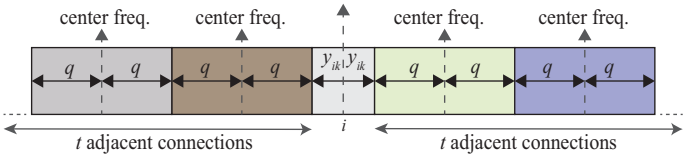

Fig. 2: Connection i at modulation format k is surrounded by $t = 2$ adjacent channels. The bandwidths of connection i and every adjacent channel is $2y_{ik}$ and $2q$, respectively.

threshold needed to satisfy the BER performance of the assigned modulation format.

According to [10] and [30, Eqs. (1) and (4)], G_{ASE_i} and G_{NLI_i} of connection i, when assigned modulation format k, can be calculated for the physical routing path r as

$$G_{\text{ASE}_i} = \sum_{l \in r} N^l G^0_{\text{ASE}} \tag{2}$$

$$G_{\text{NLI}_i} = \sum_{l \in r} N^l G^l_{\text{NLI}_i} \tag{3}$$

where

$$G^0_{\text{ASE}} = (e^{\alpha L} - 1) n_{sp} h v \tag{4}$$

$$G^l_{\text{NLI}_i} = \mu \Bigg(\underbrace{\text{asinh}(\rho \Delta f_i^2)}_{\text{SCI}} + \underbrace{\sum_{j \in A_l \setminus \{i\}} \ln \frac{\Delta f_{ij} + \Delta f_j/2}{\Delta f_{ij} - \Delta f_j/2}}_{\text{XCI}} \Bigg). \tag{5}$$

Here, G^0_{ASE} and $G^l_{\text{NLI}_i}$ are ASE and NLI noise, respectively, encountered by connection i at modulation format k on a single span on link l; N^l is the number of spans on link l along the designated path r; L is the length of each span; α is the fiber power attenuation; n_{sp} is the spontaneous emission factor; h is Planck's constant; v is the light frequency; $\mu = (3\gamma^2 G^3)/(2\pi\alpha|\beta_2|)$; $\rho = (\pi^2|\beta_2|)/(2\alpha)$; A_l is the set of all connections on link l; Δf_i is the bandwidth of connection i at its assigned modulation format; Δf_{ij} is the center frequency spacing between connections i and j; γ is the fiber nonlinearity coefficient; and β_2 is the fiber dispersion.

The two terms in (5) represent the self-channel interference (SCI) and the cross-channel interference (XCI), respectively [30]. The SCI term can be easily calculated given the connection's bit rate and the spectral efficiency of the assigned modulation format, which are independent of the actual network state. However, to calculate the XCI of a given connection, prior knowledge (i.e., the bit rate, modulation format, and spectrum) of other co-propagating channels is needed. To attain the requisite information, every link would need to be scrutinized very closely, which is both a complex and time-consuming task. Thus, we propose the following novel, low-complexity approximation method to calculate the XCI for a given connection at an assigned modulation format.

In Fig. 2, connection i at modulation format k is surrounded on each side by $t = 2$ adjacent channels or connections in a single span of an arbitrary link. The bandwidth of connection i is $2y_{ik}$ and each adjacent channel has a bandwidth of $2q$. Setting $\Delta f_j = 2q$ for all adjacent channels and $\Delta f_{ij} \in \{y_{ik} + q, y_{ik} + 3q, \ldots\}$ in the XCI term of (5) yields

$$2\mu \sum_{n=1}^{t} \ln \left[\frac{y_{ik} + 2nq}{y_{ik} + 2(n-1)q} \right]. \tag{6}$$

The worst case XCI is approximated by assigning large values to t and $2q$. In (6), we estimate t to be equal to the number of channels along the most congested link. This is found by considering the shortest routing path for every connection, as in most situations, the shortest path has the highest probability of being chosen, despite other routing possibilities. Each adjacent channel is assumed to occupy a large bandwidth (i.e., by assigning the maximum bit rate and the smallest modulation format). Therefore, $2q$ is the bandwidth for the maximum bit rate of any connection in the network when the adjacent channel is assigned the modulation format with the smallest spectral efficiency (then, $\Delta f_j/2 = q, \forall j$ in (5)).

Since G^0_{ASE} and $G^l_{\text{NLI}_i}$ can now be determined for connection i at modulation format k on a single span when the constants $\{\alpha, L, n_{sp}, h, v, G, \gamma, \beta_2\}$ are known apriori, the transmission reach for connection i at modulation format k is estimated in terms of the number of spans as

$$R_{ik} = \frac{G/\text{SNR}^k}{G^0_{\text{ASE}} + G^l_{\text{NLI}_{ik}}}. \tag{7}$$

C. Example: The impact of regenerator site selection

In this section, we explain how the selection of regenerator sites affects the spectral efficiency of an EON using an illustrative example.

Fig. 3 depicts a small 5-node EON that is required to accommodate 6 offline traffic connections. The length (i.e., number of spans) of each link is indicated beside the respective link in the same figure. Each link has a maximum capacity of 6 spectrum slots or subcarriers. Every connection can be served using modulation format 1 (Mod1) or 2 (Mod2). Mod2 is assumed to have a larger constellation. Therefore, Mod2 requires fewer spectrum slots than Mod1 to accommodate a given connection. The number of slots occupied by a connection when assigned Mod1 or Mod 2 is reported in Fig. 3(a). The reach of each connection using Mod1 or Mod2 (e.g., R_{i1} and R_{i2}) is given in Fig. 3(b). We assume that the network can only be equipped with one regenerator site. Due to a reach limitation, connection 2 has to be regenerated at node A or B. Figs. 3(c) and (d) depict how the spectrum is allocated when node A or B is a regenerator site, respectively.

In this study, spectral efficiency is measured in terms of the maximum spectrum slot (i.e., subcarrier index) required to support a certain traffic matrix. Thus, the primary objective is to minimize the maximum spectrum slot across all links. The maximum spectrum slot in Figs. 3(c) and (d) are 6 and 5, respectively, which indicate that a higher spectral efficiency can be achieved by selecting node B as a regenerator site. In Fig. 3, the regenerator site at node B converts the modulation format of connection 2 (*S*,*D*) and converts the spectrum of connection 4 (*A*,*C*) to increase the spectrum utilization of link *B*–*D* and reduce spectrum segmentation of link *B*–*C*, respectively.

(a) Traffic matrix

Connection		Nodes	# of slots with Mod 1	Mod 2
	1	*S,A*	2	1
	2	*S,D*	2	1
	3	*S,B*	1	1
	4	*A,C*	4	2
	5	*B,C*	4	2
	6	*B,D*	4	2

(b) Estimated reach

	Reach		Reach
R_{11}	10	R_{12}	7
R_{21}	10	R_{22}	7
R_{31}	11	R_{32}	8
R_{41}	7	R_{42}	5
R_{51}	7	R_{52}	5
R_{61}	7	R_{62}	5

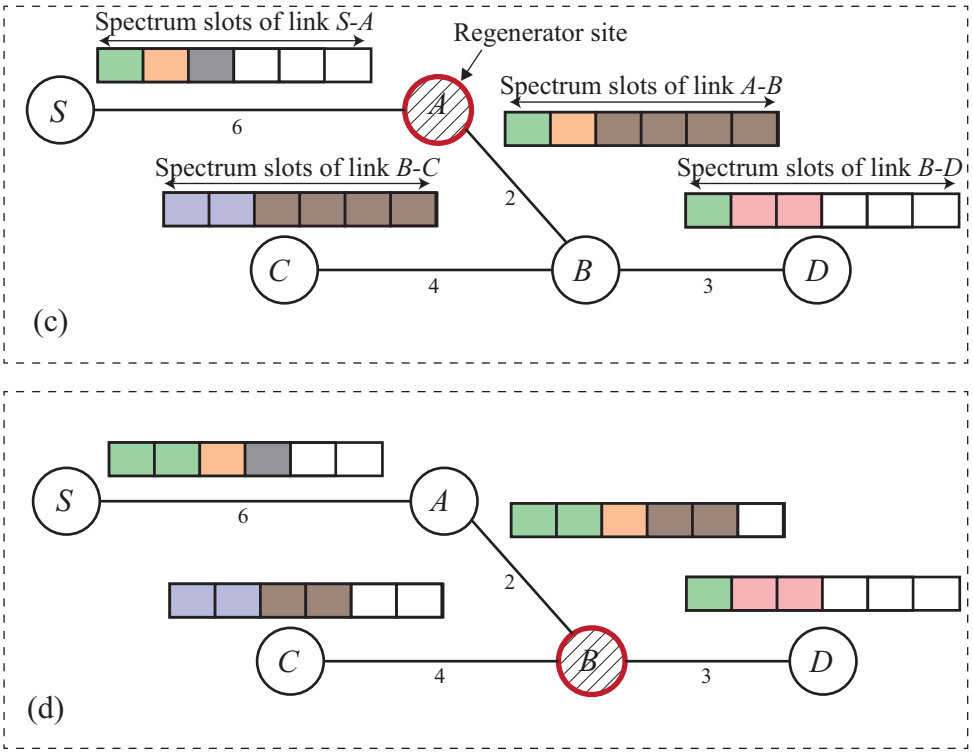

Fig. 3: Spectrum allocation in a small 5-node network serving 6 connections that is equipped with 1 regenerator site; (a) traffic matrix; (b) reach estimations of each connection at different modulation formats; (c) spectrum allocation when the regenerator site is node A; (d) spectrum allocation when the regenerator site is node B.

III. Regenerator Site Selection of an Impairment-Aware EON

Given a network with a set of nodes V, a set of links E (all links $l \in E$ have two fibers that carry traffic in opposite directions), and a set of connections T, the goal is to identify regenerator sites, perform routing, assign modulation formats, and allocate spectrum to minimize the bandwidth, quantified as the highest subcarrier index ξ assigned to any connection.

The regenerator site selection problem of an impairment-aware RSA consists of the following input parameters:

- C : The spectral width of each subcarrier.
- M : The set of modulation formats.
- c_k : The spectral efficiency of modulation format $k \in M$.
- Λ_i : The data rate (i.e., bit rate) of connection $i \in T$.
- SNR^k : The required SNR threshold of the modulation format $k \in M$.
- RG : The maximum number of regenerator sites.

We denote with s_l and d_l, respectively, the source and destination nodes of link l, which has a length of N^l (or $N^{s_l d_l}$) spans. The following parameters are predetermined using simple heuristics and the proposed XCI approximation method:

- P_i : The set of K shortest routing paths for connection $i \in T$.
- T_{ik} : The number of subcarriers required by connection i when assigned modulation format $k \in M$.
- R_{ik} : The approximated reach of connection i when assigned modulation format k according to (7).
- W_{irn} : The transparent distance to node n when connection i is routed along path $r \in P_i$.

When the above parameters are known, network operators could use the proposed algorithms to identify regenerator sites, perform routing, assign modulation formats, and allocate spectrum to maximize spectral efficiency. In the ILP formulated below, regenerator sites are identified by the binary variables Ψ_n for $\forall n \in V$. For every connection i in the connection set T, the selected routing path r among many possibilities P_i is specified by the binary variable D_{ir}. The modulation format $k \in M$ assigned to connection i on a link l along the selected routing path r is determined by the binary variable m_{irlk}. The number of subcarriers required to carry connection i on a link $l \in r$ is determined by variable B_{irl} and the lowest subcarrier index is specified by variable f_{irl}.

A. ILP formulation

The proposed ILP aims to minimize ξ by finding the optimal combination of the following variables:

a) Ψ_n : is 1 if node n is a regenerator site; else, 0.
b) D_{ir} : is 1 if connection $i \in T$ is routed along path $r \in P_i$; else, 0.
c) m_{irlk} : is 1 if connection i routed along path r and through link l is assigned modulation format k.
d) $y_{irjr'l}$: is 1 if connection i that is routed along path r and connection $j \in T$ that is routed along path $r' \in P_j$ share link l; else, 0.

e) $u_{irjr'l}$: is 1 if $y_{irjr'l} = 1$ and $f_{irl} + B_{irl} \leq f_{jr'l}$; else, 0.
f) B_{irl} : The number of subcarriers assigned to connection i on path r and through link $l \in r$.
g) f_{irl} : The lowest subcarrier index of connection i that is routed along path r and travels through link l.

The above variables should fulfil the following constraints, where θ is a large inequality coefficient ($\theta = 10^5$):

$$\sum_{n \in V} \Psi_n \leq RG \tag{8}$$

$$\sum_{r \in p_i} D_{ir} = 1, \quad \forall i \in T \tag{9}$$

$$B_{irl} \geq \sum_{k \in M} T_{ik} m_{irlk}, \quad \forall l \in r, r \in P_i, i \in T \tag{10}$$

$$\sum_{k \in M} m_{irlk} - D_{ir} = 0, \quad \forall l \in r, r \in P_i, i \in T \tag{11}$$

$$\xi \geq \quad f_{irl} + B_{irl} - 1, \quad \forall l \in r, r \in P_i, i \in T \tag{12}$$

$$\theta \Psi_n \geq f_{irl} - \sum_{z \in r \setminus \{l\}, s_z = n} f_{irz} \geq -\theta \Psi_n, \; n = d_l, \forall l \in r, r \in P_i, i \in T \tag{13}$$

$$\theta \Psi_n \geq m_{irlk} - \sum_{z \in r \setminus \{l\}, s_z = n} m_{irzk} \geq -\theta \Psi_n, \quad n = d_l, \forall k \in M, l \in r, r \in P_i, i \in T \tag{14}$$

$$W_{ird} = \begin{cases} W_{irs}(1 - \Psi_s) + N^l, & l \neq \text{ first link of } r \in P_i \\ N^l, & \text{otherwise} \end{cases} \quad d = d_l, s = s_l, \forall l \in r, r \in P_i, i \in T \tag{15}$$

$$\sum_{k \in M} m_{irlk} R_{ik} \geq \theta(D_{ir} - 1) + W_{ird}, \quad d = d_l, \forall l \in r, r \in P_i, i \in T \tag{16}$$

$$D_{ir} + D_{jr'} \leq 1 + y_{irjr'l} \tag{17}$$

$$f_{jr'l} + B_{jr'l} - f_{irl} \leq \theta(1 - y_{irjr'l} + u_{irjr'l}) \tag{18}$$

$$f_{irl} + B_{irl} - f_{jr'l} \leq \theta(1 - u_{irjr'l}) \tag{19}$$

(17)–(19) are valid $\forall l \in r \cap r', r \in P_i, r' \in P_j, \{i, j\} \in T, j \neq i$

where constraint (8) limits the number of regenerator sites; (9) ensures single-path routing; (10) and (11) specify the number of subcarriers used by a connection and its modulation format in a link; (12) guarantees that ξ is larger than the maximum subcarrier index of every connection; (13) and (14) allow the spectrum and modulation of a connection to be converted at a regenerator site; (15) determines the distance of every transparent segment; (16) guarantees that the distance in (15) is within the approximated reach of the assigned modulation format; and (17)–(19) guarantee non-overlapping spectrum allocation. A regenerator site is assumed to be able to accommodate any number of connections and, thus, the number of regenerators per site is not considered to be a constraint.

B. Proposed heuristic

The proposed ILP formulation involves many integer constraints and, thus, would only be feasible for small networks. To obtain results for larger networks, we propose the following heuristic algorithms.

In the first stage, regenerator sites are selected using Algorithm 1. The preferred routing path for each connection in Algorithm 1 is found using the balance-path-with-heavy-traffic-first algorithm in [31], which is designed to reduce the risk of overloading a single link. For each connection, we first calculate the transmission distance from every node on its preferred path to its destination node. Next, for each node, we sum the remaining transmission distances of all the connections routed via that node. For example, if only connections i and j on paths $s - x - d$ and $s - x - w - d'$, respectively, traverse node x, the summed transmission distance for node x is $N^{xd} + N^{xw} + N^{wd'}$. The nodes are then ranked in descending order of their summed value. The nodes with the highest summed values become the preferred regenerator sites. Lastly, RG regenerator sites are assigned in sequence.

In the second stage, spectrum and modulation formats are assigned to each connection along every transparent segment of the selected candidate routing path using Algorithm 2. First, connections (T) are sorted in descending order of their bit rate Λ_i. Next, the number of subcarriers in each link is initialized to zero (then $\xi = 0$). Then, starting from the first connection in the sorted list, the connections are served in a sequence. For every connection $i \in T$, a routing path r is selected from the available set P_i. If regenerator sites are present along the selected route, path r is broken into separate transparent segments at these sites. For example, if two regenerator sites are present along path r at nodes n and $n+2$, path r is broken into 3 separate segments: the source node to n, n to $n + 2$, and n to the destination node. For each segment, spectrum and modulation format are assigned accordingly. Among many possible routing paths and modulation formats, the path and modulation format that use the lowest maximum subcarrier index is chosen for every connection. Then, the values of D_{ir}, f_{irl}, B_{irl}, and m_{irlk} for the links along the chosen path are updated accordingly. If a connection cannot be routed due to the absence of spectrum, the spectrum bandwidth of each link is increased by one (i.e., ξ is increased by 1) and the simulation is repeated from the beginning.

Prior to running Algorithm 2, a test is performed to ensure that every connection can reach its respective destination node when assigned the smallest modulation format (i.e., the lowest spectral efficiency which has the longest transmission reach) and routed along the shortest path. If the test fails for any connection, the number of regenerator sites is deemed to be inadequate to serve the traffic and the algorithm comes to a halt.

The proposed heuristic algorithms include the following additional variables and functions:

Variables :

- $Cand_i$: the candidate routing path of connection i.
- $Rdist_{in}$: the transmission distance to the destination node of connection i when routed on path C_i beyond node n.
- Sum_n : the sum of the remaining distance to the destination node of every connection routed via node n.
- ϕ_i : is 1 if routing, modulation, and spectrum are assigned successfully to connection i; else, 0.
- ϱ : the maximum subcarrier index of a selected path.

Algorithm 1 : Find the regenerator sites

Inputs : $(V, E), T, P_i$.
Outputs : $\Psi_n, \quad \forall n \in V$.

Step 1: Find candidate routing paths
for $\forall i \in T$ **do**
find the candidate routing path *Cand*$_i$ of i using the BPHT algorithm
end for

Step 2: Distance after every node
for $\forall n \in V$ **do**
Sum$_n \leftarrow 0$
for $\forall i \in T$ **do**
if n is an intermediate node of C_i **then**
Rdist$_{in} \leftarrow$ transmission distance of C_i beyond node n
Sum$_n \leftarrow$ *Sum*$_n$ + *Rdist*$_{in}$
end if
end for
end for

Step 3: Regenerator site selection
Sn $\leftarrow$ nodes sorted in descending order of *Sum*$_n$
for $0 \leq x \leq \text{RG} - 1$ **do**
Let node at Sn$[x]$ be a regenerator site
$\Psi_{Sn[x]} \leftarrow 1$
end for

- κ : the maximum subcarrier index of a selected transparent segment.
- r_i : the selected routing path for connection i, $r_i \in P_i$.

Functions :

- *Len*(t) : the total number of spans along the transparent segment t.
- $ST(ik)$: is true if 1 or more T_{ik} contiguous subcarrier bands are found on every link (consisting of 0 to ξ subcarriers) in segment t; else, false.
- *Set* : the band that has the smallest maximum subcarrier index among all possible contiguous bands of size T_i^k found on every link in segment t. *Set*$[0]$ is the subcarrier index of the first spectrum slot of band *Set*.

IV. Performance evaluation

We evaluate the spectral efficiency gains of the proposed schemes using numerical simulations. Spectral efficiency gains achieved by placing regenerators at selected sites are measured against the upper bounds produced by the RIA in [10] (the connection list (CL) algorithm without regenerator sites). From a network operator's perspective, it would be interesting to know if our proposed schemes can be used to increase spectral efficiency in networks of different dimensions (e.g., size, connectivity degree) when equipped with a limited number of regenerator sites. Therefore, tests were performed on a randomly generated 6-node small network (with an average link length of 411 km), the 14-node Deutsche Telekom (DT) network [32], the 14-node National Science Foundation (NSF) network [33], [34], and the 28-node European (EU) network [33], [34] with varying numbers of regenerator sites. The respective network topologies are depicted in Figs. 4a–4c.

As previously explained, in this study, a higher spectral efficiency implies a reduced maximum subcarrier index. The

Algorithm 2 : Routing, spectrum allocation, and modulation assignment

Inputs : $(V, E), C, c_k, M, T, \Lambda_i, P_i, \text{SNR}_k$. Let $\xi \leftarrow 0$.
Outputs : $D_{ir}, f_{irl}, B_{irl}, m_{irlk}, \quad \forall l \in r, r = r_i, r_i \in P_i, i \in T$.

1: Sort T in descending order of bit rate
2: **Step 1:** Test if every connection satisfies the reach constraint.
3: **for** $\forall i \in T$ **do**
4: **for** each transparent segment t in the shortest path of i **do**
5: **if** $R_{i1} \geq$ *Len(t)* **then**
6: Exit algorithm
7: **end if**
8: **end for**
9: **end for**
10:
11: **Step 2:** Assign routing, modulation, and spectrum.
12: **Begin**
13: **for** $\forall i \in T$ **do** ▷ every connection
14: $\phi_i \leftarrow \infty, r_i \leftarrow 0$
15: **for** $\forall r \in P_i$ **do** ▷ every path
16: $\varrho \leftarrow -99$
17: **for** each transparent segment t in r **do** ▷ every segment
18: $\kappa \leftarrow \infty$
19: **for** $\forall k \in M$ **do** ▷ every mod. format
20: **if** $R_{ik} \leq$ *Len(t)* & $ST(ik) ==$ true **then**
21: *Set* $\leftarrow$ identified subcarrier set
22: **if** $\kappa \geq$ *Set*$[0] + T_{ik} - 1$ **then**
23: $\kappa \leftarrow$ *Set*$[0] + T_{ik} - 1$
24: **for** every link l in segment t **do**
25: $f_{irl} \leftarrow$ *Set*$[0]$
26: $B_{irl} \leftarrow \kappa$
27: $m_{irlk} \leftarrow k$
28: **end for**
29: **if** $\varrho \leq \kappa$ **then**
30: $\varrho \leftarrow \kappa$
31: **end if**
32: **end if**
33: **end if**
34: **end for**
35: **if** $\kappa == \infty$ **then** ▷ segment fails
36: Go to 15
37: **end if**
38: **end for**
39: **if** $\varrho \neq -99$ & $\phi_i \geq \varrho$ **then** ▷ a feasible path is found
40: $\phi_i \leftarrow \varrho, r_i \leftarrow r$
41: **end if**
42: **end for**
43: **if** $\phi_i == \infty$ **then**
44: Increase ξ by 1.
45: Go to Begin
46: **else**
47: Store the following output values,
48: $D_{i\tilde{r}} \leftarrow 1$, where $\tilde{r} = r_i$
49: $f_{i\tilde{r}l}, B_{i\tilde{r}l}$, and $m_{i\tilde{r}lk}$, for $\forall l \in \tilde{r}, \tilde{r} = r_i$
50: **end if**
51: **end for**

values assigned to the input parameters are listed in Table I. In the considered EONs, each link consists of two fibers in opposite directions. Henceforth, the proposed ILP formulation and the heuristic will be denoted as RSIE-ILP and RSIE (**r**egenerator **s**ite selection in **i**mpairment-aware **E**ONs), respectively. For each test network, simulations are repeated multiple times for random traffic matrices and the average values are reported. To reflect the heterogeneity of the Internet, connections between every node pair are assigned a random

bit rate. Unless specified otherwise, the assigned bit rate of every connection ranges between 32.5 and 130 Gb/s and the PSD G is 10 mW/THz. Three different traffic volumes are generated by assigning each connection a bit rate in the range of (i) 32.5–65 Gb/s, (ii) 32.5–130 Gb/s, and (iii) 32.5–260 Gb/s, respectively.

To evaluate the impact of different sorting policies on the performance of our proposed algorithm, RSIE is repeated by ordering the connections:

- in decreasing order of their shortest path length (RSIE-L);
- in decreasing order of $\Lambda_i \times$ shortest path length (RSIE-BL).

Also, to perform comparisons, the results of RSIE is evaluated against the results of modified weighted MLR-combined algorithm (WMC) proposed in [17]. As WMC was designed for mixed-line-rate WDM networks, it had to be modified to be applicable to EONs. The modified WMC algorithm for an EON consists of two stages. In the first stage, it selects the regenerator sites using an extended version of the approximation algorithm presented in [12]. Every connection i is routed via the shortest routing path r_i. We estimated the maximum transmission reach ϱ_k for every modulation format k to be $\lfloor G/(\mathrm{SNR}^k G^0_{\mathrm{ASE}}) \rfloor$ spans at PSD G. The transmission reach ϱ_k is rounded to the closest odd number.

Next, the modified WMC algorithm selects a given number RG of regenerator sites by generating the following triplets and sets:

1) (v, i, k) : A triplet indtactes that node v is situated along the designated path r_i of connection i, which is assigned modulation format k.
2) $AT = \{(v, i, k) | v \in r_i, i \in T, k \in M\}$: AT is a set that includes all triplets.
3) $PV_v = \{r_i | i \in T, v \in r_i\}$: PV_v includes the routing paths of all connections that travel through node v.
4) For every path $r_i \in PV_{v^1}$, for every node $v^* \in r_i$, for every modulation format k, set b_v includes all triplets $(v^*, i, k) \in AT$ such that at least one of the following conditions is satisfied:
   a) The distance between node v^* and node v is less than or equal to $(\varrho_k - 1)/2$.
   b) The distance between the source node of the connection i and node v along path r_i is less than or equal to ϱ_k, and node v^* is situated between the source node and v.
   c) The distance between the destination node of the connection i and node v along path r_i is less than or equal to ϱ_k, and node v^* is situated between the destination node and v.
5) Select as regenerator sites the RG nodes $v \in V$ with largest $|b_v|$. For example, if $RG = 2$ and $|b_{v^1}| > |b_{v^3}| > |b_{v^n}|$, then b_{v^1} and b_{v^3} are selected and their corresponding nodes (e.g nodes v^1 and v^3) are set as regenerator sites.

Finally, routes, spectrum, and modulation formats are assigned to each connection using Algorithm 2.

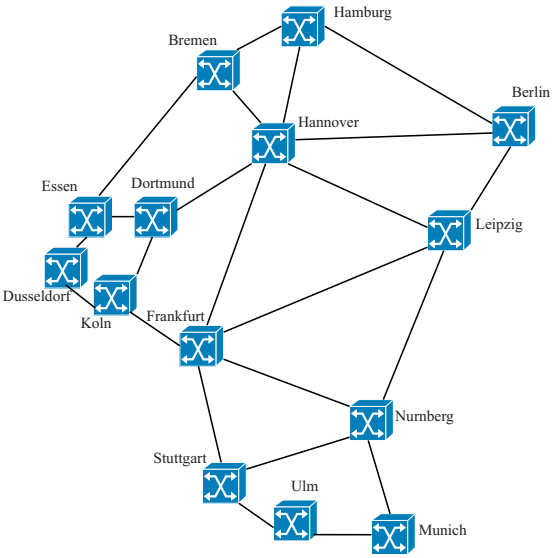

(a) DT network topology

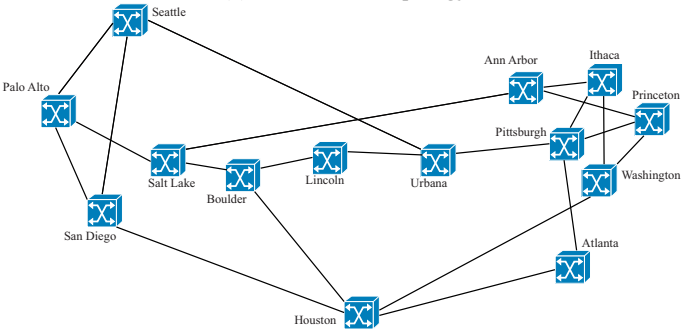

(b) NSF network topology

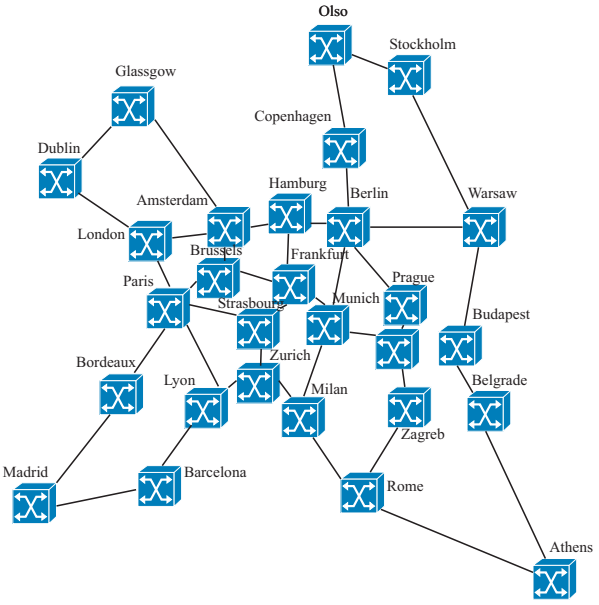

(c) EU network topology

Fig. 4: Network topologies

TABLE I: Values assigned to the parameters [10], [35]

Parameter	Value
α	0.22 dB/km
γ	1.3 (W km)$^{-1}$
β_2	-21.7ps^2/km
n_{sp}	1.8
v	93 THz
L	100 km
M	{1,2,3,4} b/s/Hz
BER requirement	10^{-3}
C	6.25 GHz

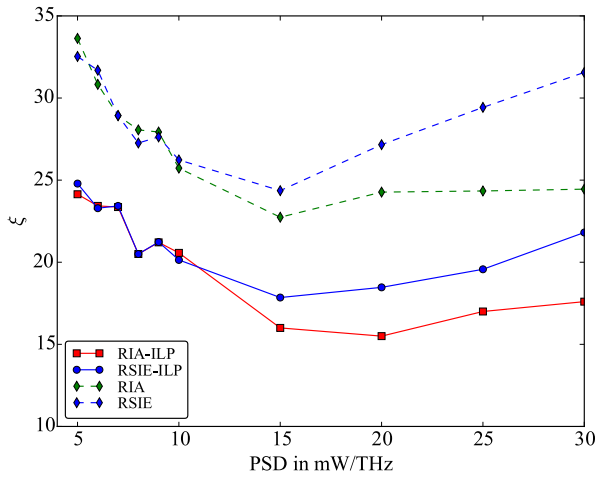

Fig. 5: Maximum subcarrier index vs. PSD for the RSIE-ILP, RSIE, RIA-ILP, and RIA schemes in the 6-node network without regenerators.

A. Validity of the approximation method

First, we ascertain if the proposed approximation method provides comparable results to the actual GN model. To perform this analysis, we compare the results of RSIE-ILP and RSIE (which use the approximation method) against RIA (which uses the actual GN model) for the small 6-node network without any regenerator sites (RG $= 0$). In Fig. 5, the maximum subcarrier indices of the proposed RSIE-ILP, RSIE, RIA-based ILP (RIA-ILP), and RIA-based heuristic (RIA) are plotted against increasing PSD. As expected, RSIE-ILP and RIA-ILP offer higher spectral efficiency over the RSIE and RIA heuristic algorithms. When PSD G is smaller than 10 mW/THz, the results of RSIE-ILP and RSIE are quite similar to that of RIA-ILP and RIA, respectively. Even when the PSD is increased to 15 mW/THz, RSIE-ILP and RSIE only consume 10% and 6% more subcarriers than RIA-ILP and RIA, respectively. This indicates that when the PSD is small, the approximation method provides comparable results to the actual GN model. However, at higher PSD values, the approximation method offers somewhat lower spectral efficiency for the reason that it finds the worst-case PLI value and, thus, overestimates the impairments when the PSD is large.

In Fig. 6, we compare the maximum subcarrier index of RSIE against RIA for the large 14-node DT network at different traffic volumes. Although a slight difference in results

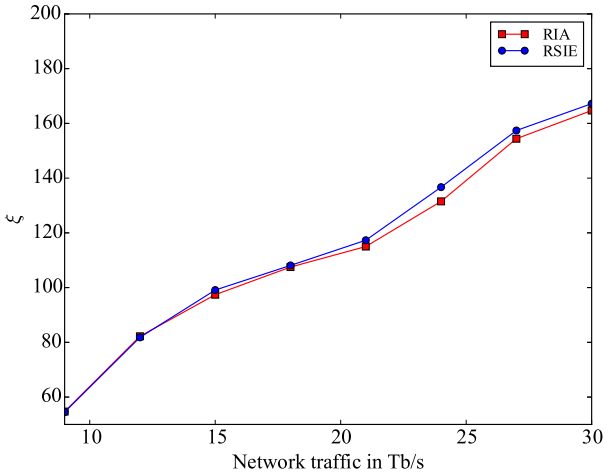

Fig. 6: Maximum subcarrier index vs. different network traffic volumes for RSIE and RIA in the DT network without regenerators.

is observed at higher traffic volumes (a maximum difference of 4%), in general, RSIE and RIA produce comparable results at all traffic volumes. Based on these observations, we conclude that the approximation method provides a good estimation of XCI for both large and small networks at all traffic volumes if the PSD is small.

B. Spectral efficiency increase

1) Small 6-node network: The performance of RSIE-ILP and RSIE is evaluated in terms of the achieved reduction in maximum subcarrier index with a given number of regenerator sites. While RSIE-ILP can be used to attain optimal results for small networks, RSIE is used to provide suboptimal results for large networks. In Fig. 7, we compare the performance of RSIE-ILP and RSIE in the small 6-node network at three different traffic volumes and against an increasing number of regenerator sites. RSIE-ILP provides the highest performance at all traffic volumes, which is especially true at high traffic volumes. Although the performance of RSIE-ILP and RSIE can be improved by adding more regenerator sites, such performance gains diminish after a certain threshold.

2) 14-node DT network: In Fig. 8, the maximum subcarrier index of RSIE is plotted against an increasing number of regenerator sites for three different traffic volumes in the 14-node DT network. In this figure, RSIE increases spectral efficiency by approximately 24%, 21%, and 30% via placing 3, 5, and 6 regenerator sites in the DT network when the traffic volume is (i) low, (ii) intermediate, and (iii) high, respectively. Similar to the results in Fig. 7, the performance gains diminish when the number of regenerator sites in the network is increased beyond a certain threshold. This trend indicates that even with a limited number of regenerator sites, the proposed RSIE algorithm can achieve spectral efficiency gains in a large network at different traffic volumes. However, spectral efficiency can be significantly improved by employing

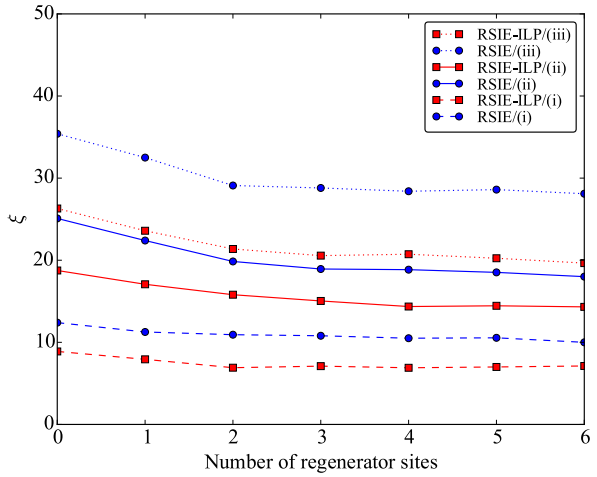

Fig. 7: Maximum subcarrier index vs. increasing number of regenerator sites for RSIE-ILP and RSIE in the DT network.

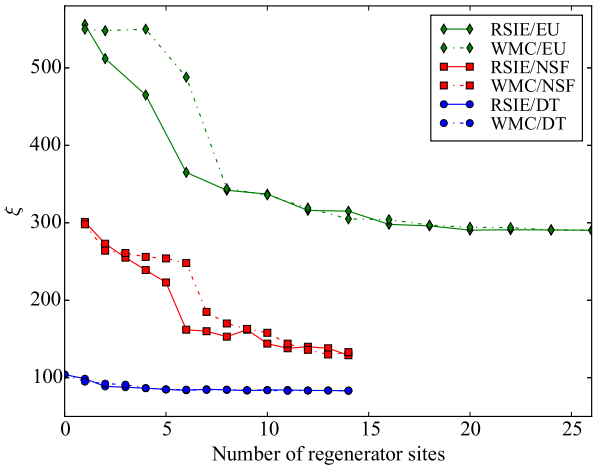

Fig. 9: Maximum subcarrier index vs. increasing number of regenerator sites for RSIE in the DT, NSF, and EU networks.

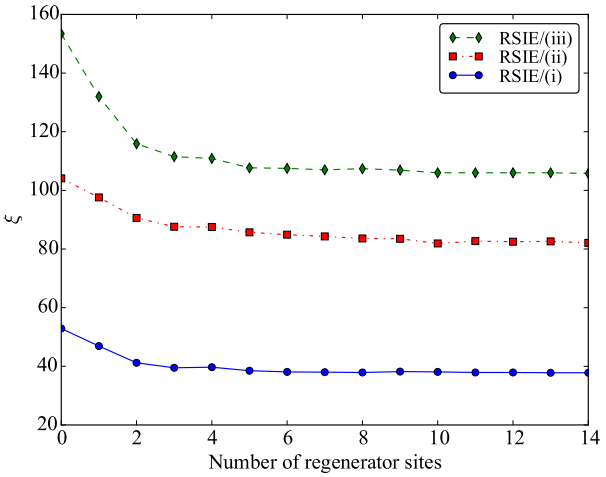

Fig. 8: Maximum subcarrier index vs. increasing number of regenerator sites at different traffic volumes in the DT network.

more regenerator sites when the network is serving a large traffic volume.

C. Network size

In Fig. 9, we compare the spectral efficiency gains of our proposed scheme in networks of different sizes. Fig. 9 also includes the results obtained by the WMC algorithm. Network size is measured in terms of link length, the number of nodes, and the degree of connectivity. The plotted results indicate that the spectral efficiency gains of RSIE is significant in the NSF and EU networks. Although both the DT and NSF networks have an identical number of core nodes, the links of the NSF network are much longer. As a result, traffic connections have to travel further distances in the NSF network. Connections that travel a long distance (i.e., more spans) encounter severe impairments. Although its links are relatively short, the EU network has more core nodes and, thus, a large number of connections travel through its links. Consequently, nonlinear impairments due to XCI is much larger in the EU network. Therefore, regenerators play an equally critical role in both the NSF and EU networks. On the other hand, as the DT network is smaller (i.e., fewer core nodes and shorter links), regenerators play a limited role in this network. As results are plotted as an average over multiple simulations (multiple random traffic matrices), it was observed that the NSF and EU networks had to be equipped with at least 2 and 1 regenerator sites, respectively, to accommodate most traffic matrices. By appropriately placing regenerator sites, RSIE increases spectral efficiency gains in the DT, NSF, and EU networks by approximately 20%, 30%, and 46%, respectively. It is also observed that the spectral gains become negligible in DT, NSF, and EU networks when the number of regenerator sites exceed 5, 9, and 20, respectively. Based on these results, we conclude that our proposed scheme provides significant spectral efficiency gains in large networks, especially when the network contains a large number of core nodes.

For the DT network, RSIE and WMC produce similar results. However, for the NSF and EU networks, we observe that RSIE consumes less spectrum than WMC when the network is equipped with a lower number of regenerators. Specifically, RSIE can save up to 32% and 25% spectrum compared with WMC in the NSF and EU networks, respectively.

D. Regenerator sites

To demonstrate the superiority of our regenerator site selection Algorithm 1, in Fig. 10, we compare the results of RSIE against the results obtained by randomly selecting the regenerator sites. Additionally, we include the results of RSIE-L, RSIE-BL, WMC, and RIA (the regenerators were placed using Algorithm 1). The simulations were performed on the 14-node DT network. For all test algorithms, the results produced a similar trend. As mentioned earlier, RSIE and WMC show comparable results and offer higher spectral efficiency gains than RSIE-L, RSIE-BL, and the result of random site

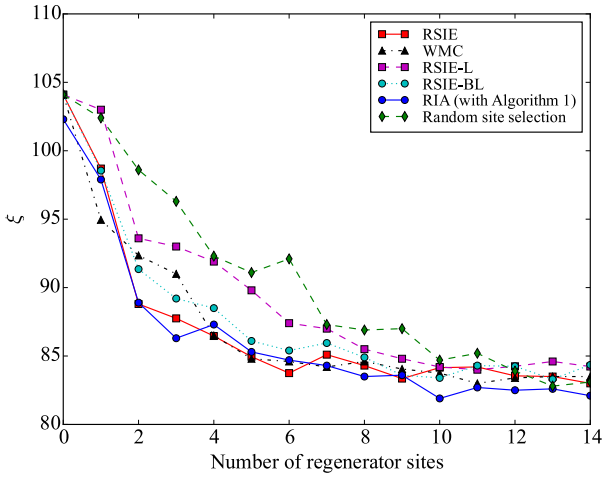

Fig. 10: Maximum subcarrier index vs. increasing number of regenerator sites for RSIE and RIA schemes with different sorting algorithms in the DT network.

selection. This indicates that bit-rate-based connection sorting policy produces higher spectrum savings than other two sorting policies. RIA (using 1) offers marginal spectrum efficiency improvements over RSIE when the network is equipped with a large number of regenerators as it more accurately approximates the nonlinear impairments. Specifically, spectral efficiency can be increased by up to 11% when Algorithm 1 is used compared with a random selection of sites.

After repeating the simulations for each network with random traffic matrices of different traffic volumes and different RG values, in Fig. 11, we depict the probability of a node becoming a regenerator site (calculated by dividing the number of times the node was selected as a regenerator by the total number of simulations) in the DT, NSF, and EU networks. For example, the results depicted in Fig. 11a were generated after repeating the simulation with 20 random traffic matrices for each traffic volume ((i), (ii), and (iii)), and for every RG value from 1 to 14. In the DT network, Leipzig, Frankfurt, and Hannover are most often selected as regenerator sites (probability > 0.8). In the NSF network, Houston, Seattle, and Pittsburgh have a higher probability of being selected as regenerator sites. Berlin, Frankfurt, Munich, and Paris are the most common regenerator sites in the EU network. Based on these results, it is our opinion that core nodes that have a higher degree of connectivity and are commonly used as intermediate nodes by connections that travel a long distance are often suitable as regenerator sites. On the other hand, core nodes that predominantly serve local traffic (i.e., edge core nodes) are rarely selected as regenerator sites. In both the DT and EU networks, Frankfurt serves as an intermediate node for a large number of long-reach connections and has a higher connectivity degree (5 or 4). Thus, Frankfurt is chosen as a regenerator site in both networks. On the other hand, Berlin and Munich, which are chosen as regenerator sites in the EU network, are seldom selected in the DT network as they have a low degree of connectivity and serve mostly local traffic. This indicates that regenerator site selection strongly depends on the network topology.

V. Conclusions

To alleviate signal degradation and increase transmission reach, optical connections at times have to be regenerated at intermediate nodes. To reduce network cost, it is preferable to have only a few regenerator sites. Existing work addressing the regenerator site selection problem in EONs have not considered a realistic PLI model and, thus, they do not accurately gauge the effect of regenerator sites. To overcome this significant limitation, a novel regenerator site selection scheme for impairment-aware EONs was proposed in this study. The primary objective was to increase spectral efficiency by appropriately selecting regenerator sites, which was formulated as an ILP and a heuristic. Through numerical simulations, we demonstrated that by appropriately selecting a few regenerator sites, spectral efficiency can be considerably increased in different-sized networks at different traffic volumes. Specifically, the spectral gains of our proposed scheme is significant in large networks and at large traffic volumes. Our study finally highlights the key characteristics of potential regenerator sites of a given network.

References

[1] Cisco Systems Inc., "Cisco visual networking index: forecast and methodology, 2014-2019," pp. 1–14, 2015.

[2] K. Christodoulopoulos, I. Tomkos, and E. A. Varvarigos, "Elastic bandwidth allocation in flexible OFDM-based optical networks," *Journal of Lightwave Technology*, vol. 29, no. 9, pp. 1354–1366, 2011.

[3] M. Jinno, H. Takara, B. Kozicki, Y. Tsukishima, Y. Sone, and S. Matsuoka, "Spectrum-efficient and scalable elastic optical path network: architecture, benefits, and enabling technologies," *IEEE Communications Magazine*, vol. 47, no. 11, pp. 66–73, 2009.

[4] J. Zhang, Y. Ji, M. Song, X. Yu, J. Zhang, and B. Mukherjee, "Dynamic traffic grooming in sliceable bandwidth-variable transponder-enabled elastic optical networks," *Journal of Lightwave Technology*, vol. 33, no. 1, pp. 183–191, 2015.

[5] Z. Fan, Y. Qiu, C.-k. Chan, and S. Member, "Dynamic multipath routing with traffic grooming in OFDM-based elastic optical path networks," *Journal of Lightwave Technology*, vol. 33, no. 1, pp. 275–281, 2015.

[6] J. Zhang, Y. Zhao, X. Yu, J. Zhang, M. Song, Y. Ji, and B. Mukherjee, "Energy-efficient traffic grooming in IP-over-elastic optical networks," *Journal of Optical Communications and Networking*, vol. 7, no. 1, pp. A142–A152, 2015.

[7] G. Zhang, M. De Leenheer, and B. Mukherjee, "Optical traffic grooming in OFDM-based elastic optical networks," *Journal of Optical Communications and Networking*, vol. 4, no. 11, pp. B17–B25, 2012.

[8] X. Chen, Y. Zhong, and A. Jukan, "Multipath routing in elastic optical networks with distance-adaptive modulation formats," in *IEEE International Conference on Communications (ICC)*. Budapest, Hungary, 2013, pp. 3915–3920.

[9] M. Jinno, B. Kozicki, H. Takara, A. Watanabe, Y. Sone, T. Tanaka, and A. Hirano, "Distance-adaptive spectrum resource allocation in spectrum-sliced elastic optical path network," *IEEE Communications Magazine*, vol. 48, no. 8, pp. 138–145, 2010.

[10] J. Zhao, H. Wymeersch, and E. Agrell, "Nonlinear impairment-aware static resource allocation in elastic optical networks," *Journal of Lightwave Technology*, vol. 33, no. 22, pp. 4554–4564, 2015.

[11] M. Flammini, G. Monaco, L. Moscardelli, M. Shalom, and S. Zaks, "Optimizing regenerator cost in traffic grooming," *Theoretical Computer Science*, vol. 412, no. 52, pp. 7109–7121, 2011.

[12] M. Flammini, A. Marchetti-Spaccamela, G. Monaco, L. Moscardelli, and S. Zaks, "On the complexity of the regenerator placement problem in optical networks," *IEEE/ACM Transactions on Networking*, vol. 19, no. 2, pp. 498–511, 2011.

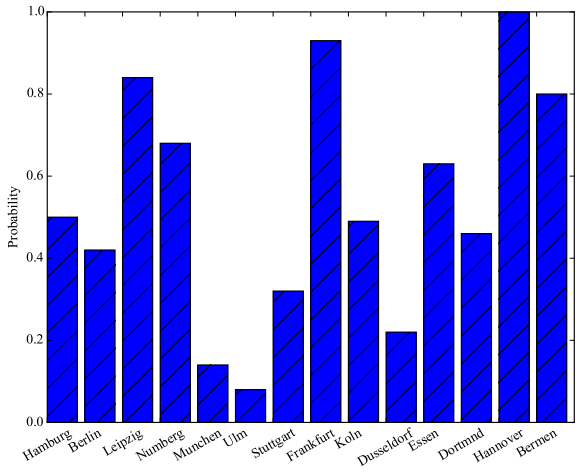

(a) DT network

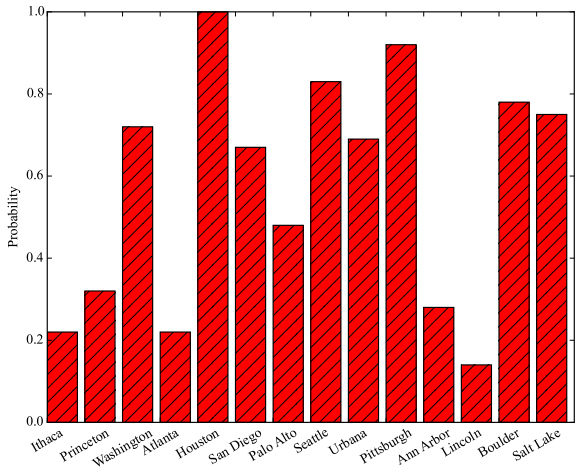

(b) NSF network

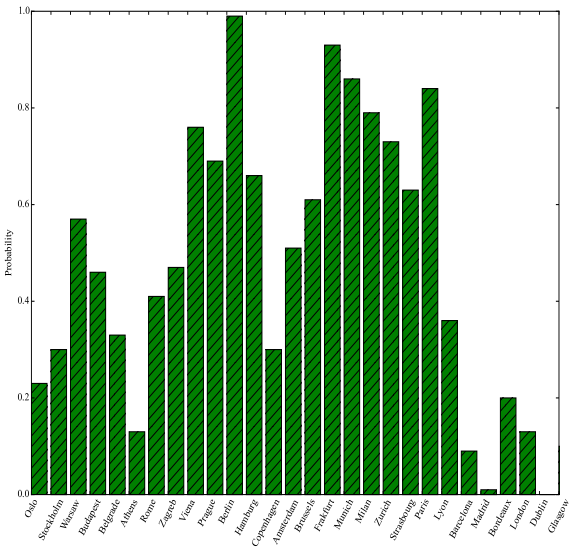

(c) EU network

Fig. 11: The probability of core nodes in different cities being selected as regenerator sites. These probabilities are found after repeating the simulation with multiple random traffic matrices of different traffic volumes ((i), (ii), (iii)) and with all possible RG values.

[13] F. Kuipers, A. Beshir, A. Orda, and P. Van Mieghem, "Impairment-aware path selection and regenerator placement in translucent optical networks," in *International Conference on Network Protocols (ICNP)*, 2010.

[14] S. Varma and J. P. Jue, "Regenerator placement and waveband routing in optical networks with impairment constraints," in *IEEE International Conference on Communications (ICC)*, Kyoto, Japan, 2011.

[15] S. Varma and J. Jue, "Regenerator site selection in mixed line rate waveband optical networks," *Journal of Optical Communications and Networking*, vol. 5, no. 3, pp. 198–209, 2013.

[16] A. N. Patel, C. Gao, J. P. Jue, X. Wang, Q. Zhang, P. Palacharla, and T. Naito, "Cost efficient traffic grooming and regenerator placement in impairment-aware optical WDM networks," *Optical Switching and Networking*, vol. 9, no. 3, pp. 225–239, 2012.

[17] W. Xie, J.P. Jue, X. Wang, Q. Zhang, Q. She, P. Palacharla, and M. Sekiya, "Regenerator site selection for mixed line rate optical networks," *Journal of Optical Communications and Networking*, vol. 6, no. 3, pp. 391–309, 2014.

[18] W. Xie, J.P. Jue, "Cost-optimized design of flexible-grid optical networks considering regenerator site selection," in *Global Communications Conference (GLOBECOM)*, 2013, pp. 2358–2363.

[19] M. Klinkowski, "On the effect of regenerator placement on spectrum usage in translucent elastic optical networks," in *International Conference on Transparent Networks (ICTON)*, Coventry, U.K., 2012.

[20] S. Yang and F. Kuipers, "Impairment-aware routing in translucent spectrum-sliced elastic optical path networks," in *17th European Conference on Networks and Optical Communications (ECOC)*, 2012.

[21] A. Kahya, "Routing, spectrum allocation and regenerator placement in flexible-grid optical networks," Ph.D. dissertation, 2013. [Online]. Available: http://www.thesis.bilkent.edu.tr/0006572.pdf

[22] A. Fallahpour, H. Beyranvand, S. A. Nezamalhosseini, and J. A. Salehi, "Energy efficient routing and spectrum assignment with regenerator placement in elastic optical networks," *Journal of Lightwave Technology*, vol. 32, no. 10, pp. 2019–2027, 2014.

[23] M. Aibin and K. Walkowiak, "Adaptive modulation and regenerator-aware dynamic routing algorithm in elastic optical networks," in *IEEE International Conference on Communication*, London, U.K., 2015, pp. 5138–5143.

[24] D. A. R. Chaves, E. F. Silva, C. J. A. Bastos-Filho, and H. A. Pereira, "Heuristic algorithms for regenerator assignment in dynamic translucent elastic optical networks," in *International Conference on Transparent Networks (ICTON)*, Budapest, Hungary, 2015, p. We.B1.2.

[25] X. Wang, M. Brandt-Pearce, and S. Subramaniam, "Impact of wavelength and modulation conversion on transluscent elastic optical networks using MILP," *Journal of Optical Communications and Networking*, vol. 7, no. 7, pp. 644–655, 2015.

[26] A. Klekamp, R. Dischler, and F. Buchali, "Limits of spectral efficiency and transmission reach of optical-OFDM superchannels for adaptive networks," *IEEE Photonics Technology Letters*, vol. 23, no. 20, pp. 1526–1528, 2011.

[27] P. Johannisson and E. Agrell, "Modeling of nonlinear signal distortion in fiber-optical networks," *Journal of Lightwave Technology*, vol. 32, no. 23, pp. 4544–4552, 2014.

[28] S. Zhang, Y. Ji, M. Song, Y. Zhao, J. Zhang, and B. Mukherjee, "Dynamic traffic grooming in sliceable bandwidth-variable transponder-enabled elastic optical networks," *IEEE Journal on Selected Areas in Communications*, vol. 33, no. 1, pp. 183–191, 2015.

[29] P. Poggiolini, "The GN model of non-linear propagation in uncompensated coherent optical systems, vol. 30, no. 24, pp. 3857–3879, 2012.

[30] L. Yan, E. Agrell, H. Wymeersch, and M. Brandt-Pearce, "Resource allocation for flexible-grid optical network with nonlinear channel model," *Journal of Optical Communications and Networking*, vol. 7, no. 11, pp. B101–B108, 2015.

[31] C. Xiaojun, V. Anand, Y. Xiong, and C. Qiao, "A study of waveband switching with multilayer multigranular optical cross-connects," *IEEE Journal on Selected Areas in Communications*, vol. 21, no. 7, pp. 1081–1095, 2003.

[32] M. Angelou, Y. Pointurier, D. Careglio, S. Spadaro, and I. Tomkos, "Optimized monitor placement for accurate QoT assessment in core optical networks," *Journal of Optical Communications and Networking*, vol. 4, no. 1, pp. 15–23, 2012.

[33] R. Hulsermann, S. Bodamer, M. Berry, A. Betker, C. Guager, M. Jager, M. Kohn, and J. Spath, "A set of typical transport network scenarios for network modelling," in *5th ITG Workshop on Photonic Networks*, Leipzig, Germany, 2004, pp. 65–71.

[34] A. Betker, C. Gerlach, R. Hulsermann, M. Jager, M. Barry, S. Bodamer, J. Spath, C. Gauger, and M. Kohn, "Reference

transport network scenarios," Tech. Rep., 2003. [Online]. Available: http://wall.ikr.uni-stuttgart.de/printable/Content/IKRSimLib/Usage/Referenz_Netze_v14_full.pdf

[35] T. Tanaka, A. Hirano, and M. Jinno, "Advantages of IP over elastic optical networks using multi-flow transponders from cost and equipment count aspects." *Optics Express*, vol. 22, no. 1, pp. 62–70, Jan. 2014.